Evaluation of Force Fields for Molecular Simulation of Polyhedral Oligomeric Silsesquioxanes

Tudor C. Ionescu,[†] Feng Qi,[‡] Clare McCabe,*[,†] Alberto Striolo,[†] John Kieffer,[‡] and Peter T. Cummings[†,§]

Department of Chemical Engineering, Vanderbilt University, Nashville, Tennessee 37235-1604, Department of Materials Science and Engineering, University of Michigan, Ann Arbor, Michigan 48109, and Chemical Sciences Division, Oak Ridge National Laboratory, Oak Ridge, Tennessee 37831-6224

Received: May 23, 2005; In Final Form: November 4, 2005

Polyhedral oligomeric silsesquioxanes (POSS) are nanometer-size molecules suitable for the production of organic−inorganic nanocomposite materials. These organic−inorganic nano-building blocks show promise for enabling the production of polymeric materials of exceptional mechanical properties as well as novel composite materials. While the experimental studies of these materials have rapidly evolved in the past decade, their theoretical investigation is still in its infancy. Toward the validation of force fields for the molecular simulation of POSS-containing systems, we present the charge-transfer reactive (CTR) force field for the molecular simulation of polyhedral oligomeric silsesquioxane (POSS) molecules and compare the ability of this, and several force fields taken from the literature, to predict the thermophysical properties of POSS-containing systems. The literature force fields compared include the universal force field (UFF) and the COMPASS and Hybrid-COMPASS force fields. Predictions from molecular dynamics simulations of the structural parameters (unit cell vectors), melting temperature, and FT-IR spectra of crystals of POSS monomers are presented. The POSS monomers investigated are octahydride, octamethyl, and octapropyl POSS. Predicted quantities are compared to experimental results where available and provide molecular-level physical insight into several aspects of the behavior of POSS molecules. While all the force fields tested perform reasonably well, our results indicate that the Hybrid-COMPASS and CTR force fields predict structural properties that are in good agreement with experimental data.

1. Introduction

Polyhedral oligomeric silsesquioxanes (POSS) are multifunctional molecules, with the chemical composition $(RSiO_{1.5})_n$ (n = 4, 6, 8, 10...) which is intermediate between that of silica (SiO_2) and polysiloxanes $(R_2SiO)_n$. The most-studied members of the series are the octasilsesquioxanes (n = 8), which have a cube-shaped Si_8O_{12} core with organic groups R at each corner. Figure 1 shows the simplest member of the octasilsesquioxane family, the polyhedral octahydridosilsesquioxane ($H_8Si_8O_{12}$), often referred to as T8, in which the organic groups are hydrogen atoms. Because of the rich chemistry of these molecules, POSS-based systems have a wide range of potential applications, for example, as additives to paints, coatings, packaging materials, resins, elastomers, and advanced plastics, where they enhance the abrasion and temperature resistance, increase the glass transition temperature, and improve mechanical properties (without compromising processibility).[1,2]

The first experimental studies on POSS-containing systems focused on determining the crystal structures of a variety of POSS monomers[3−5] and was followed by work from several groups to solve the crystal structures of other octasubstituted silsesquioxanes $R_8Si_8O_{12}$, with R = $-C_2H_3$,[6] $-CH_3$,[7] $-Cl$,[8] and $-nC_3H_6I$.[9] More recently, Waddon et al. investigated the crystal structure of a cyclopentyl−POSS−norbornenyl monomer (containing seven cyclopentyl and one norbornenyl groups),[10,11] which is a widely used POSS monomer in composite applications; the seven chemically inert cyclopentyl groups help dissolve the POSS unit into a polymer matrix, while the one chemically reactive norbornyl group acts as a site for further polymerization or grafting reactions.

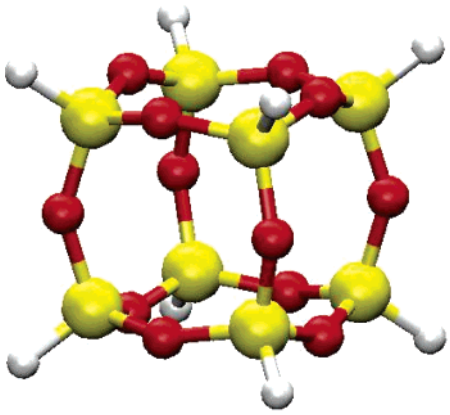

Figure 1. Schematic representation of octahydridosilsesquioxane ($H_8Si_8O_{12}$). Hydrogen atoms are colored in white, silicon atoms are colored in yellow, and oxygen atoms are colored in red.

In recent years, significant research efforts have focused on the development of POSS molecules as molecular nanoscale building blocks for the production of nanocomposite materials. The outstanding feature of polyhedral silsesquioxanes, in

* Corresponding author. E-mail: c.mccabe@vanderbilt.edu. Telephone: (615) 322-6853. Fax: (615) 343-7951.
[†] Department of Chemical Engineering, Vanderbilt University.
[‡] Department of Materials Science and Engineering, University of Michigan.
[§] Chemical Sciences Division, Oak Ridge National Laboratory.

10.1021/jp052707j CCC: $33.50
Published on Web 01/26/2006

contrast to that of traditional silsesquioxanes, is the perfect monodispersity of cage shape and size that, coupled with the unique ability to independently functionalize each corner of a POSS cube with different organic or inorganic groups, confers a nearly infinite array of possible nanostructures made of assemblies of POSS molecules. Additionally POSS monomers are relatively inexpensive and readily available in large (>1 tonne/yr) monodisperse quantities (in contrast, nanotubes are expensive and produced in small quantities). Several experimental studies have examined the effect of POSS monomers on the mechanical and thermal properties of a variety of polymers.[12,13] Some authors report that the reinforcing effect of the POSS units is due to their aggregation into microdomains, while others attribute the enhancement of the composite properties to the bulkiness of the POSS monomers without invoking their aggregation.

To properly understand and control the aggregation and crystallization of monomers in POSS-based nanocomposites, it is necessary to fully understand the thermodynamic and mechanical properties of POSS cubes and the interactions that occur between POSS monomers at a molecular level. Given the limited availability of experimental techniques that probe such details, molecular simulation appears to be the ideal tool to gain this understanding. However, while powerful algorithms to study thermodynamic and mechanical properties of polymeric materials have been developed, the results obtained are only reliable if realistic expressions for the force fields that describe the interactions between the atoms and molecules in the system are included in the calculations. To permit the study of POSS monomers by molecular simulation, we have developed a new force field and compare this force field to others taken from the literature in the prediction of the crystal structures of several POSS monomers. X-ray diffraction patterns computed from the simulation results are compared to experimental data where available. In addition, we have calculated densities and diffusion coefficients for POSS monomers as a function of temperature and estimated the melting temperature. The remainder of the paper is organized as follows: in Section 2, we provide a detailed description of the force fields used in this work, and in Section 3, we give details of the simulations performed. In Section 4, we discuss the simulation results obtained with the different force fields studied, and compare our predictions to the available experimental data. Finally, in Section 5, we summarize our findings.

2. Methods and Force Fields

Several force fields have been evaluated for describing POSS molecules: the universal force field (UFF),[14] the condensed-phase optimized molecular potentials for atomistic simulation studies force field (COMPASS), a simplified version of COMPASS,[15,16] referred to as Hybrid-COMPASS (HC), and the new charge-transfer reactive (CTR) force field. In earlier work, on the basis of ab initio calculations, we demonstrated that when an alkane tether is substituted for one organic group R on the POSS cage, the geometrical features of both the POSS cage and the alkane tether do not significantly change when compared to the isolated molecules. Thus, we concluded that it should be possible to describe the properties of alkane-substituted POSS monomers by combining force fields independently developed to describe alkane chains and siloxane molecules.[17] Hence, for simulations of alkyl-functionalized POSS cages, we have combined the force fields chosen to described silsesquioxane molecules with a well-established alkane force field, namely the transferable potential for phase equilibria united atom force field (TraPPE UA).[18] In what follows, we briefly summarize the main features of each of the force fields used in this work.

2.1. Universal Force Field (UFF). In the UFF force field, the total potential energy U is given by

$$U = U_b + U_\theta + U_\Phi + U_{vdw} \quad (1)$$

where U_b represents the bond-stretching interactions, U_θ represents the angle-bending interactions, U_Φ represents the torsional interactions, and U_{vdw} represents the nonbonded interactions. The bond-stretching interaction can be described either as a harmonic oscillator or as a Morse function. In this work, the harmonic oscillator formulation is used:

$$U_b = 1/2k_{IJ}(r - r_{IJ})^2 \quad (2)$$

where r_{IJ} is the equilibrium bond length between atoms I and J, r is the actual bond length between atoms I and J, and k_{IJ} is the force constant. The angle-bending term is described as a harmonic cosine oscillator:

$$U_\theta = 1/2k_\theta(\cos\theta - \cos\theta_0)^2 \quad (3)$$

where θ_0 is the equilibrium angle, θ is the actual angle, and k_θ the force constant. The torsional interactions are given by a cosine potential,

$$U_\Phi = A[1 + \cos(m\Phi - \delta)] \quad (4)$$

where A is a constant, m the periodicity coefficient, Φ the dihedral angle, and for the force field considered here, $\delta = 0$. The nonbonded interactions between atoms in different molecules and between atoms in the same molecule but separated by three or more bonds are described by a 12−6 Lennard−Jones potential:

$$U_{vdw} = \epsilon_{IJ}\left\{-2\left[\frac{r_{IJ}}{r}\right]^6 + \left[\frac{r_{IJ}}{r}\right]^{12}\right\} \quad (5)$$

where ϵ_{IJ} represents the depth of the potential well, r_{IJ} is the distance between the atoms when the energy is a minimum (i.e., $U_{vdw} = -\epsilon_{IJ}$), and r is the actual distance between the atom pair $I-J$. The parameters $\epsilon_{II} \equiv \epsilon_I$ and $r_{II} \equiv r_I$ are tabulated for like atom pairs, while the unlike atom interactions are determined by using the geometric combining rules

$$r_{IJ} = (r_I r_J)^{1/2} \quad (6)$$

$$\epsilon_{IJ} = (\epsilon_I \epsilon_J)^{1/2} \quad (7)$$

In Table 1, we report all the parameters used to implement the UFF force field for the POSS systems studied.

2.2. Condensed-Phase Optimized Molecular Potentials (COMPASS) and Hybrid-COMPASS Force Fields (HC). In the COMPASS force field, the total potential energy U is given by,

$$U = U_b + U_\theta + U_\phi + U_\chi + U_{bb'} + U_{b\theta} + U_{b\phi} + U_{\theta\phi} + U_{b\theta\phi} + U_{coul} + U_{vdw} \quad (8)$$

The terms on the right-hand side of eq 8 can be divided into two categories: valence terms, which include bond-stretching (U_b), bond-angle-bending (U_θ), torsion (U_Φ), out-of-plane angle-bending (U_χ), cross-coupling terms (bond−bond ($U_{bb'}$), bond−

TABLE 1: Parameters Used in the UFF Force Field for the POSS Monomers Studied

E_b	k_{IJ} (kcal/mol Å^2)	r_{IJ} (Å)
Si−H	345.4464	1.4705
Si−O	879.8471	1.5917
E_θ	k (kcal/mol)	θ_0 (deg)
H−Si−O	104.06	109.47
Si−O−Si	440.91	146.0
O−Si−O	300.08	109.47
E_{vdw}	ϵ_{IJ} (kcal/mol)	r_{IJ} (Å)
Si−Si	0.402	4.295
Si−O	0.155306	3.8771
Si−H	0.13299	3.5207
O−O	0.060	3.500
O−H	0.05138	3.17827
H−H	0.044	2.886
E_φ	A (kcal/mol)	δ (deg)	m
H−Si−O−Si	0.0742	0.0	3.0
Si−O−Si−O	0.0742	0.0	3.0

angle ($U_{b\theta}$), bond−torsion ($U_{b\Phi}$), and bond−angle−torsion ($U_{b\theta\Phi}$) interactions), and nonbonded interaction terms, which include the Coulombic function (U_{coul}) for electrostatic interactions and the Lennard−Jones 9−6 function (U_{vdw}) for van der Waals interactions. The full COMPASS force field was used in this work as implemented in Materials Studio.[19] A simplified version of the COMPASS force field, in which the out-of-plane angle-bending and the cross-coupling interaction terms are neglected, has also been tested. We refer to this latter force field as Hybrid-COMPASS (HC). In the HC potential, the bond-stretching U_b and angle-bending U_θ terms are described by quartic functions

$$U_b = k_2(b - b_0)^2 + k_3(b - b_0)^3 + k_4(b - b_0)^4 \quad (9)$$

$$U_\theta = H_2(\theta - \theta_0)^2 + H_3(\theta - \theta_0)^3 + H_4(\theta - \theta_0)^4 \quad (10)$$

where b_0 is the equilibrium bond length and θ_0 the equilibrium bond angle, b the actual bond length, θ the actual angle, and H_2, H_3, H_4 and k_2, k_3, and k_4 are constants. The torsion term U_Φ is given by the triple cosine function,

$$U_\Phi = V_1(1 - \cos(\Phi)) + V_2(1 - \cos(2\Phi)) + V_3(1 - \cos(3\Phi)) \quad (11)$$

where Φ is the actual value of the dihedral angle, and V_1, V_2, and V_3 are constants. The electrostatic interactions are described by the Coulombic function,

$$U_{coul} = \sum_{I,J} \frac{q_I q_J}{r_{IJ}} \quad (12)$$

where q_I and q_J represent the partial charges of atoms I and J, respectively, and r_{IJ} is the distance between atoms I and J. The partial charges on each atom are computed using the method of bond increments, as implemented in COMPASS by Sun.[20] For atom i, the partial charge is given by

$$q_I = \sum_J \delta_{IJ} \quad (13)$$

where the sum is of all charge bond increments δ_{IJ} (which are tabulated values) for atoms J that are valence bonded to atom I. The van der Waals interactions are described by the Lennard−Jones 9−6 potential function,

$$U_{vdw} = \epsilon_{IJ}\left\{2\left[\frac{r_{IJ}}{r}\right]^9 - 3\left[\frac{r_{IJ}}{r}\right]^6\right\} \quad (14)$$

where ϵ_{IJ} represents the depth of the potential well, r_{IJ} is the distance between the atoms where $U_{vdw} = -\epsilon_{IJ}$, and r is the actual distance between the atom pair. The van der Waals potentials are calculated for every nonbonded atom pair within a cutoff radius, usually 10 Å, and for atoms separated by two or more bonds on the same chain. The Lennard−Jones parameters ϵ_{IJ} and r_{IJ} are tabulated for like atom pairs. For unlike atom pairs, a 6th order combining rule is used to calculate the parameters,

$$r_{IJ} = \left(\frac{r_I^6 + r_J^6}{2}\right)^{1/6} \quad (15)$$

$$\epsilon_{IJ} = \left(\frac{2r_I^3 r_J^3 \sqrt{\epsilon_I \epsilon_J}}{r_I^6 + r_J^6}\right) \quad (16)$$

where r_I, r_J, ϵ_I, and ϵ_J represent the like atom interaction parameters for atoms I and J, respectively. In Table 2, we report all the parameters used to implement the Hybrid-COMPASS force field in this work.

TABLE 2: Parameters Used in the Hybrid-COMPASS Force Field for the POSS Monomers Studied

E_b	b_0 (Å)	k_2 (kcal/mol Å^2)	k_3 (kcal/mol Å^3)	k_4 (kcal/mol Å^4)
Si−O	1.64	350.1232	−517.3424	673.7067
Si−H	1.478	202.78	−305.36	280.27
Si−C	1.899	189.65	−279.42	307.51
E_θ	θ_0 (deg)	H_2 (kcal/mol rad^2)	H_3 (kcal/mol rad^3)	H_4 (kcal/mol rad^4)
Si−O−Si	159.0	8.500	−13.4188	−4.1785
O−Si−O	110.7	70.3069	−6.9375	0.0
H−Si−O	107.4	57.6643	−10.6506	4.6274
C−Si−O	114.9	23.0218	−31.3993	24.9814
E_φ		V_1 (kcal/mol)	V_2 (kcal/mol)	V_3 (kcal/mol)
Si−O−Si−O		−0.225	0	−0.010
Si−O−Si−H		0.0	0.0	−0.010
Si−O−Si−C		0.0	0.0	−0.010
E_{vdw}		r_{IJ} (Å)		ϵ_{IJ} (kcal/mol)
Si4−Si4		4.405		0.198
Si4−Si4c		4.3494		0.16054
Si4−O		4.0323		0.08993
Si4−H		3.9737		0.03492
Si4−C		4.1744		0.09063
Si4c-Si4c		4.290		0.131
Si4c−O		3.9437		0.0771
Si4c−H		3.8779		0.03037
Si4c−C		4.1007		0.0856
O−O		3.300		0.080
O−H		3.1241		0.03951
O−C		3.6290		0.06342
H−H		2.878		0.0230
H−C		3.5262		0.0268
C−C		3.8540		0.0620

2.3. Charge-Transfer Reactive (CTR) Force Field. The CTR force field was originally conceived for the study of inorganic materials with mixed ionic and covalent bonding, and an earlier version has proven successful in reproducing the

TABLE 3: Parameters Used in the CTR Force Field for the POSS Monomers Studied

element	σ (Å)	NN
Si	0.101	4
O	0.143	2
H	0.065	1

pair	A_{ij} (10^{-19} J)	ρ_{ij} (nm^{-6})	λ_{ij} (nm)	η_{ij} (nm)	κ_{ij} (nm^{-1})	r_{ij} (nm)	C_{ij} (Jm^{-1})
Si−Si	0.10	34.50	0	0	34.50	0	0
Si−O	0.05	45.12	0	3.2	45.12	0.1600	0
Si−H	0.10	56.20	0	3.0	56.20	0.1515	0
O−O	0.10	30.50	0	0	30.50	0	0
O−H	0.48	80.50	0	3.0	80.50	0	0
H−H	0.10	34.50	0	0	34.50	0	0

charge transfer	δ_{ij} (e)	a (nm)	b (nm^{-1})
Si−O	−0.1940	0.20	57
Si−H	−0.0230	0.19	75

triplet	γ_{ijk} (rad^{-2})	θ (rad)
O−Si−O	0.21	1.911
O−Si−H	0.49	1.911
Si−O−Si	0.19	2.591

structural transition between various silica polymorphs with a single parametrization.[21] The use of this potential in the present context was motivated by the inorganic character of the core of the polyhedral octahydridosilsesquioxane ($H_8Si_8O_{12}$) building blocks. The CTR force field has been parametrized to reproduce the stable crystal structure and vibrational properties of the POSS cage. The CTR force field includes a Coulomb term, U_{Cb}, a Born−Huggins−Mayer repulsive term, U_{BMH}, a three-body term, U_{3B}, and an attractive van der Waals term U_{vdw}. giving the following expression for the total energy:

$$U_{total} = U_{Cb} + U_{BMH} + U_{3B} + U_{vdw} \tag{17}$$

The Coulomb interaction between point charges is expressed as

$$U_{Cb} = \frac{1}{4\pi\epsilon_0}\sum_{j\neq i}^{N}\frac{q_i q_j}{r_{ij}} \tag{18}$$

The long-range aspects of these interactions are treated by using the Ewald summation method. The fractional point charge on atom i is given by $q_i = -2\sum_{j=1}^{NN}\delta_{ij}\zeta_{ij}$, where $\zeta_{ij} = (e^{(r_{ij}-a)b} + 1)^{-1}$ controls the transfer of charge between atoms i and j, δ_{ij} is the total amount of transferable charge, a and b are constants, and r_{ij} is the distance between atoms i and j. The van der Waals interactions are given by,

$$U_{vdw} = -\sum_{j\neq i}^{N}\frac{C_{ij}}{r_{ij}^6} \tag{19}$$

where C_{ij} is a constant. The repulsion between atomic cores is modeled by the Born−Mayer−Huggins term according to

$$U_{BMH} = \sum_{j\neq i}^{N} A_{ij}\left(1 + \frac{z_i}{n_i} + \frac{z_j}{n_j}\right)e^{(\sigma_i+\sigma_j-r_{ij})\cdot\rho_{ij}} \tag{20}$$

where A_{ij} is the preexponential energy scaling factor, ρ_{ij} is the hardness parameter, z_i is the valence electron number, and n_i is the number of outer shell electrons. The parameter σ_i provides a measure of the atom size. The three-body term accounts for the directionality of covalent bonds by constraining the angle between two adjacent bonds. This term is conditional upon the existence of covalent attraction between atoms and is given by

$$U_{3B} = \sum_{j=1}^{NC-1}\sum_{k=j+1}^{NC}(\varphi_{ij} + \varphi_{jk})\, e^{-\gamma_{ijk}(\theta_{ijk}-\theta_0)^2} \tag{21}$$

where θ is the angle formed by the $i-j$ and $i-k$ bonds, and φ is an angular spring constant,

$$\varphi_{ij} = -A_{ij}\left(1 + \frac{z_i}{n_i} + \frac{z_j}{n_j}\right)\frac{\kappa_{ij}}{\eta_{ij}}\zeta_{ij}\, e^{\lambda_{ij}}\, e^{-r_{ij}\eta_{ij}} \tag{22}$$

where η_{ij}, λ_{ij}, and κ_{ij} are empirical constants. For torsional interactions, the expression for U_Φ given by eq 11 has also been implemented in this force field. In Table 3, we report the parameters used to implement the CTR force field.

2.4. TraPPE Force Field. The TraPPE UA force field specifies that the total energy U has the same functional form as the UFF model (eq 1). The bond-stretching and bond-angle-bending interactions are modeled as harmonic oscillators, as given by

$$U_b = 1/2k_{IJ}(r - r_{IJ})^2 \tag{23}$$

$$U_\theta = 1/2k_\theta(\theta - \theta_0)^2 \tag{24}$$

The terms in eq 23 are defined as in eq 2. In eq 24, θ_0 is the equilibrium value of the angle, θ is the actual value, and k_θ is a constant. The torsional potential U_Φ is given by a triple cosine function,

$$U_\Phi = c_1[1 + \cos(\Phi)] + c_2[1 - \cos(2\Phi)] + c_3[1 + \cos(3\Phi)] \tag{25}$$

where Φ is the actual value of the dihedral angle, and c_1, c_2, and c_3 are constants. The *nonbonded* interaction term U_{vdw} is given by the Lennard−Jones 12−6 LJ potential function

$$U_{vdw} = 4\epsilon_{IJ}\left\{\left[\frac{\sigma_{IJ}}{r}\right]^{12} - \left[\frac{\sigma_{IJ}}{r}\right]^{6}\right\} \tag{26}$$

The unlike atom interactions are determined by using the Lorenz−Berthelot combining rules,

$$\sigma_{IJ} = (\sigma_I + \sigma_J)/2 \tag{27}$$

$$\epsilon_{IJ} = \sqrt{\epsilon_I\epsilon_J} \tag{28}$$

For alkyl-functionalized POSS molecules, the cross nonbonded van der Waals interactions are treated by following the work of Frischknecht and Curro.[22] The Si−C bond-stretching potential from the HC force field was used to determine the Si−CH_2 and Si−CH_3 bond-stretching potentials. Similarly, the O−Si−C HC angle-bending potential was used for the O−Si−CH_2 and O-Si−CH_3 interactions, and the HC X−Si−C−X torsion potential was used to represent the O−Si−CH_2−CH_2 torsional potential. In Table 4, we report the parameters used to implement the TraPPE force field in this work, and in Table 5, the van der Waals nonbonded cross interactions for alkyl-POSS systems.

3. Simulation Details

Molecular dynamics simulations were carried out using the public domain DL_POLY 2 code,[23] the Accelrys Materials

TABLE 4: Parameters Used in the TraPPE Force Field for the Alkyl-POSS Monomers Studied with the Hybrid-COMPASS (HC) Force Field

E_b	k_{IJ} (kcal/mol Å^2)	r_{IJ} (Å)
C−C	889.9	1.540
E_θ	k (kcal/mol)	θ_0 (deg)
C−C−C	124.3122	114.0
E_{vdw}	e_{IJ} (kcal/mol)	r_{IJ} (Å)
CH_3-CH_3	0.194921	3.7500
CH_3-CH_2	0.133544	3.8500
CH_2-CH_2	0.091493	3.9500
E_φ	c_1 (kcal/mol)	c_2 (kcal/mol)	c_3 (kcal/mol)
C−C−C−C	1.4123	−0.27126	3.14786

TABLE 5: Parameters Used for the Cross Nonbonded Interactions in the Description of Alkyl-POSS Molecules with the Hybrid-COMPASS (HC) and TraPPE Force Fields

	ϵ_{IJ} (kcal/mol)	σ_{IJ} (Å)
$Si-CH_2$	0.10947	3.886
$Si-CH_3$	0.15960	3.830
$O-CH_2$	0.08550	3.445
$O-CH_3$	0.12470	3.380

Studio software package,[19] and an in-house code, FLX. Crystal structures were simulated by using the Berendsen constant pressure algorithm[24] with the Rahman−Parrinello anisotropy correction[25] when using DL_POLY 2, and the Rahman−Parrinello constant pressure algorithm when using FLX and Materials Studio. In both cases, not only the volume, but also the shape of the simulation box, is allowed to vary. In all the simulations, an integration time step of 1 fs was used. For simulations performed with Materials Studio and FLX, bonded and nonbonded interactions were evaluated at every time step. To increase computational efficiency in DL_POLY 2, a multiple time step method was employed in which the bonded interactions were evaluated at every time step, and the nonbonded interactions evaluated every five time steps. The starting unit cell fractional coordinates were obtained from Larson[3,26] and Heyde[3,26] for $H_8Si_8O_{12}$, and from Larson[4] for $(CH_3)_8Si_8O_{12}$. In both cases, the crystal arrangement is hexagonal, with the unit cell containing three molecules. The simulation box contained $4 \times 4 \times 2$ unit cells for a total of 96 molecules in the $H_8Si_8O_{12}$ case, and $3 \times 3 \times 2$ unit cells for a total of 54 molecules in the $(CH_3)_8Si_8O_{12}$ case. The structures were first equilibrated for 500 ps at 100 K for $H_8Si_8O_{12}$ and at 300 K for $(CH_3)Si_8O_{12}$, and then data were collected from several 100 ps to 500 ps production runs. For the simulations performed to study the melting of the crystal, after each 100 ps run, the temperature was increased by 100 K. This procedure was repeated until the structures were observed to melt.

4. Results

We first focus on the results of the structural calculations. We computed via molecular mechanics simulations the molecular structure of the POSS cage predicted from the different force fields to compare with experimental data and ab initio calculations.[17] Bond lengths and angles were measured and averaged over the course of each molecular mechanics simulation for the different force fields considered. The results are presented in Table 6 for polyhedral octahydridosilsesquioxane, T8. The results indicate that the predictions obtained by using standard force fields satisfactorily reproduce the available experimental data. Because of the computationally intensive nature of electrostatic interactions in a force field, we also performed calculations using the Hybrid-COMPASS force field with the electrostatic interactions turned off (referred to as HC w/o). We note from the results that the prediction of the molecular structure of octahydridosilsesquioxane monomers ($H_8Si_8O_{12}$) with the HC force field is in good agreement with the experimental data both with and without the inclusion of electrostatic interactions in the force field. This is perhaps not unexpected, given that the partial charges in the HC force field are small. Because the calculation of electrostatic interactions is computationally expensive, this is an advantageous feature of the HC force field.

TABLE 6: Molecular Structure Predictions for $H_8Si_8O_{12}$ from the CTR, UFF, COMPASS, HC, HC w/o Force Fields Compared with Experimental Values

	CTR	UFF	COMPASS	HC	HC w/o	expt[a]
Si−O (Å)	1.620	1.5896	1.624	1.6702	1.6383	1.619
Si−H (Å)	1.4760	1.4637	1.473	1.4819	1.4761	1.4805
Si−O−Si (deg)	146.80	147.00	146.95	146.7	146.86	147.54
O−Si−O (deg)	109.73	109.92	110.19	110.26	110.09	109.6

[a] Reference 26.

Although no experimental data is available to confirm our findings, it is instructive to study the POSS cage with alkyl tethers through molecular mechanics simulations to study the impact of the tethers on the cage structure.[17] The effect of substituting all eight hydrogen atoms with propyl chains is presented in Table 7 for the UFF, COMPASS, and HC w/o force fields. As suggested by previous ab initio calculations of monotethered POSS cages, this has minimal impact on the cage structure. Furthermore, we note that the results from the three different force fields are consistent in that the Si−O bond lengths and the Si−O−Si angle show a slight increase, while the O−Si−O angle shows a slight decrease in propyl POSS compared to T8 POSS in all cases.

Having validated the use of UFF, COMPASS, HC, and CTR force fields to satisfactorily reproduce the intramolecular structural parameters of POSS monomers, we now turn to the prediction of the crystal structure. Crystalline structures were investigated for T8 POSS ($H_8Si_8O_{12}$) and polyhedral octamethyl silsesquioxane ($(CH_3)_8Si_8O_{12}$). In Figure 2, we report representative simulation snapshots for the $H_8Si_8O_{12}$ crystal at 100 K and the $(CH_3)_8Si_8O_{12}$ crystal at 300 K. The hexagonal unit cell, used to initialize the simulations, was in each case conserved during the simulation, in agreement with experimental data.[5,10] In Table 8, we report the predicted crystal structure parameters for the $H_8Si_8O_{12}$ crystal at 100 K and 300 K, and for the $(CH_3)_8Si_8O_{12}$ crystal at 300 K from the different force fields alongside the experimental values. Our results show that the UFF force field overestimates the experimental crystal density by approximately 10% for all systems considered. The CTR potential also overestimates the crystal density, which is believed to be caused by the lack of a LJ repulsive term. For both the octahydrido and octamethyl POSS crystals, the best prediction for the crystal density and unit cell dimensions is given by HC force field. We again note that the differences arising from excluding the electrostatic interactions are minimal.

The simulated crystal structures have also been compared to experiment[3,4,26] using X-ray diffraction analysis. X-ray diffraction patterns were calculated using atomic fractional coordinates from the final simulation configurations at different temperatures. X-ray diffraction patterns for $H_8Si_8O_{12}$, obtained from our simulations at 100 K and 300 K, are compared to those obtained from experimental crystallographic data in Figures 3 and 4, respectively. For all the force fields used, the description

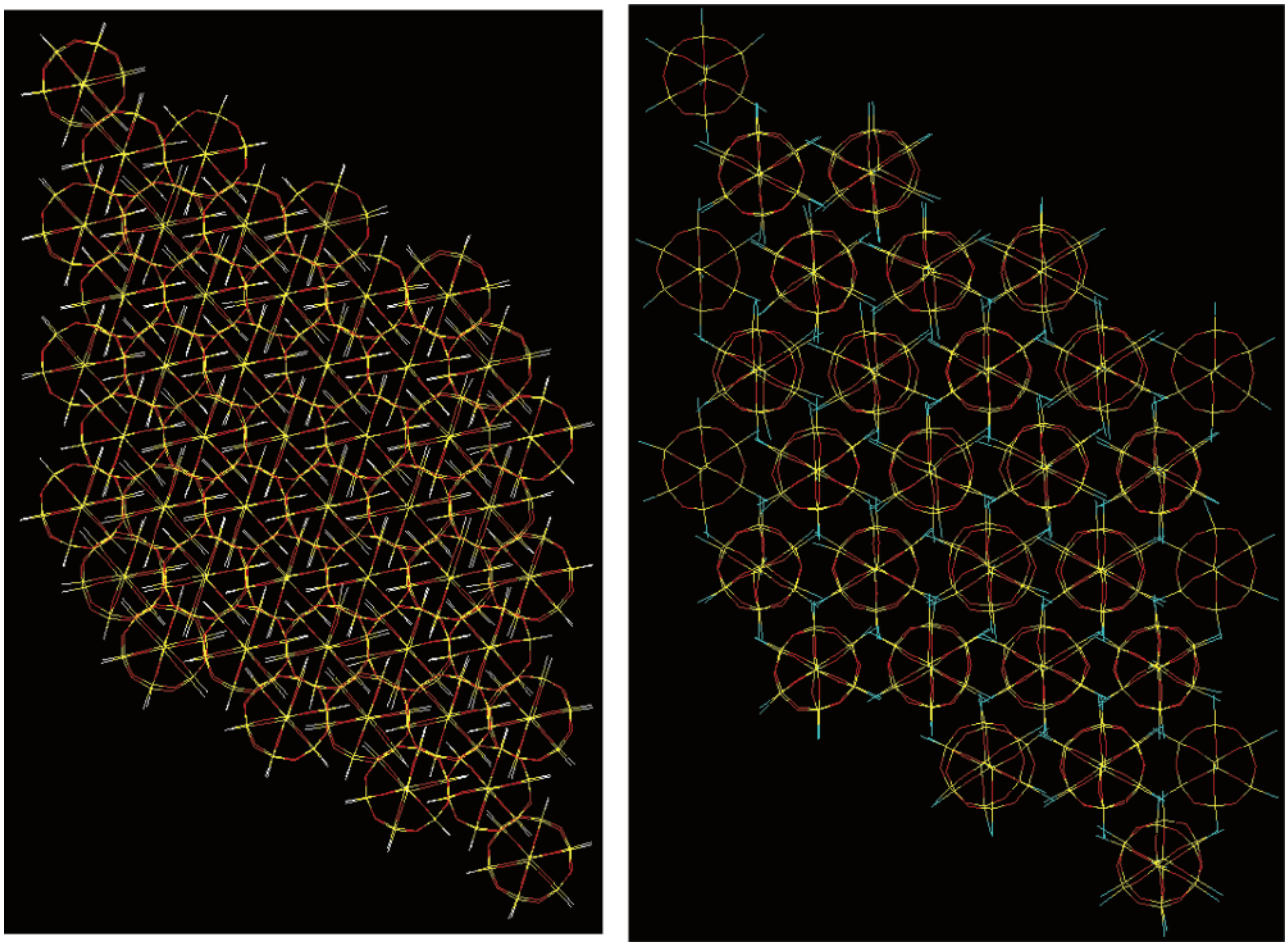

Figure 2. Simulation snapshots of (a) $H_8Si_8O_{12}$ at 100 K and (b) $(CH_3)_8Si_8O_{12}$ at 300 K obtained using the HC w/o force field.

TABLE 7: Effect of Substituting the Hydrogen Atoms on the POSS Cage with a Propyl Tether on the Structure of the Cage; Comparisons Are Made Between the UFF, COMPASS, and HC w/o Force Fields

	UFF		COMPASS		HC w/o	
	$H_8S_{18}O_2$	$(CH_3CH_2CH_2)Si_8O_{12}$	$H_8S_{18}O_2$	$(CH_3CH_2CH_2)Si_8O_{12}$	$H_8S_{18}O_2$	$(CH_3CH_2CH_2)Si_8O_{12}$
Si(1)−O(2) (Å)	1.590	1.593	1.624	1.633	1.639	1.642
Si(1)−O(2)−Si(3) (deg)	147.00	151.00	147.95	150.17	146.86	150.63
O(2)−Si(3)−O(4) (deg)	109.90	108.40	110.19	108.39	110.09	107.00

TABLE 8: Comparison of the Predicted Crystal Structure Parameters for the $H_8Si_8O_{12}$ Crystal at 100 K and 300 K from the UFF, HC, HC w/o, and CTR Force Fields, and for the $(CH_3)_8Si_8O_{12}$ Crystal at 300 K from the UFF, HC, and HC w/o Force Fields Alongside Experimental Data

	$H_8Si_8O_{12}$ 100 K			$H_8Si_8O_{12}$ 300 K			$(CH_3)_8Si_8O_{12}$ 300 K		
	ρ (g/cm^3)	a (Å)	c (Å)	ρ (g/cm^3)	a (Å)	c (Å)	ρ (g/cm^3)	a (Å)	c (Å)
UFF	2.164	8.67	15.016	2.131	8.70	15.119	1.655	12.05	12.838
HC	1.998	8.88	15.476	1.950	8.95	15.598	1.489	12.49	13.313
HC w/o	2.041	8.84	15.292	1.988	8.91	15.456	1.522	12.40	13.189
CTR	2.0683	8.74	15.55	2.044	8.76	14.49			
expt	1.97[a]	9.04[a]	15.16[a]	1.91[b]	9.13[b]	15.35[b]	1.51[c]	12.59[c]	13.08[c]

[a] Reference 26. [b] Reference 3. [c] Reference 4.

of the crystal structure is good, with the UFF force field again giving the least accurate description compared to experiment. We note that the observed shift of diffraction peaks toward higher 2θ values is a direct consequence of a higher density in the simulations compared to experiment; the relative intensities and spacing between peaks is similar in all diffraction patterns, indicating that the placement of the atoms in the unit cell is adequately reproduced by all the force fields. In Figure 5, simulated X-ray diffraction patterns are compared to experiment for $(CH_3)_8Si_8O_{12}$ at 300 K. The simulated crystal structures are in this case in excellent agreement with experiment, with the results obtained by using the UFF potential model again showing the greatest deviation from the experimental data.

Finally, in determining the suitability of different force fields to model the POSS cage, we have studied their melting properties to compare with the experimental data reported by Larsson and co-workers.[3] At the melting point, the thermodynamic properties of the system, such as density, enthalpy, and self-diffusion coefficients, show discontinuous behavior due to the first-order nature of the transition. Thus, the melting point,

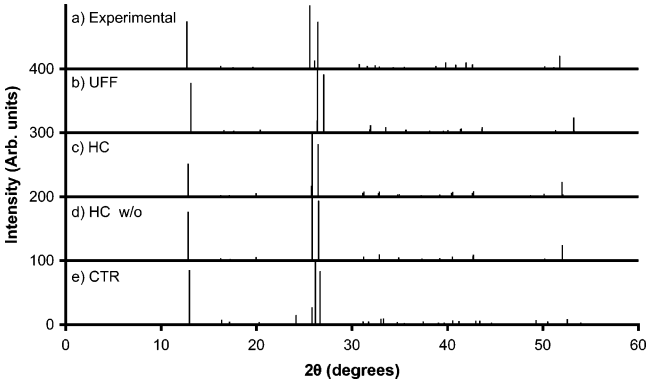

Figure 3. X-ray diffraction patterns for $H_8Si_8O_{12}$ at 100 K obtained from the different force fields studied compared with experimental data. (a) Experimental,[26] (b) simulation using UFF, (c) simulation using HC, (d) simulation using HC w/o, and (e) simulation using CTR.

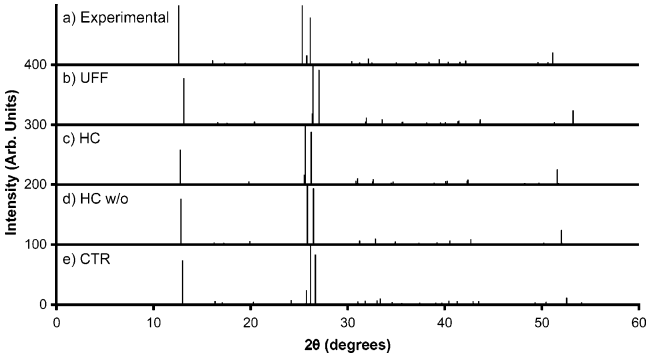

Figure 4. X-ray diffraction patterns for $H_8Si_8O_{12}$ at 300 K obtained from the different force fields studied compared with experimental data. (a) Experimental,[3] (b) simulation using UFF, (c) simulation using HC, (d) simulation using HC w/o, and (e) simulation using CTR.

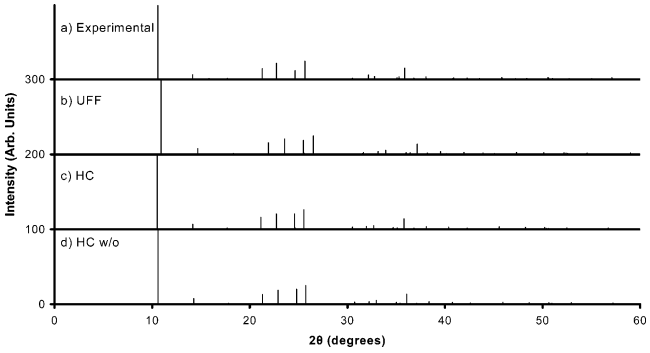

Figure 5. X-ray diffraction patterns for $(CH_3)_8Si_8O_{12}$ at 300 K. (a) Experimental,[4] (b) simulation using UFF, (c) simulation using HC, and (d) simulation using HC w/o.

T_{mp}, can be determined by calculating the above-mentioned thermodynamic quantities as functions of temperature. The self-diffusion coefficients were computed using the Einstein formula:[24]

$$D = \lim_{t\to\infty} \frac{1}{6}\frac{d}{dt}\langle|\mathbf{r}_i(t) - \mathbf{r}_i(0)|^2\rangle \qquad (29)$$

where D is the center of mass self-diffusion coefficient, $\mathbf{r}_i(0)$ are the positions of the centers of mass at the time origins, and $\mathbf{r}_i(t)$ are the positions of the centers of mass at time t. The self-diffusion coefficient for a solid is on the order of 10^{-13} m^2/s, whereas for a liquid, it is on the order of 10^{-9} m^2/s. We have also determined the translational order parameter $\rho(\mathbf{k})$,[24]

$$\rho(\mathbf{k}) = \frac{1}{N}\sqrt{(\sum_1^N \cos(\mathbf{k}\cdot\mathbf{r}_i))^2 + (\sum_1^N \sin(\mathbf{k}\cdot\mathbf{r}_i))^2} \qquad (30)$$

where N is the number of molecules in the system, $\mathbf{k}$ is a reciprocal lattice vector and $\mathbf{r}_i$ are the positions of the centers of mass of the POSS molecules. The translational order parameter $\rho(\mathbf{k})$ has a value of 1 for a perfectly ordered crystal and a value of 0 for a disordered liquid.

In Figures 6−8, we report results for the density (Figure 6), the translational order parameter (Figure 7), and the self-diffusion coefficient (Figure 8) as a function of temperature for the $H_8Si_8O_{12}$ crystal obtained from the different force fields studied. We first note that for each of the properties studied, the UFF force field indicates the melting temperature to be in excess of 1000 K, which significantly overestimates the experimental value of 523 K.[3] The results from both the HC and HC w/o force fields are generally in close agreement with each other and overestimate the experimental value. The CTR force field yields a significantly lower melting temperature than that of the other force fields, despite the fact that it overestimates the density. Presumably, the long-range electrostatic interactions, which include attraction and repulsion, dominate when the crystal expands, and a symmetry-breaking perturbation that favors the long-range repulsive interactions leads to the collapse of the structure. Similar calculations have been performed to determine the melting temperature of the $(CH_3)_8Si_8O_{12}$ and $(CH_3CH_2CH_2)_8Si_8O_{12}$ crystals with the HC w/o force field; the melting point is observed to decrease as the chain length of the alkane tether increases, in agreement with experimental measurements.[27] A simple interpretation of this melting point behavior is that the tethers increasingly screen the electrostatic interactions between the cubes as the tether length increases. We are currently performing additional simulations to confirm this conclusion.

Determining melting transitions by using molecular simulation is not a trivial task.[28] The results reported in this work used perfect, defect-free crystals, whereas real crystals have defects and surfaces that have been shown to initiate melting.[29] Therefore, we would anticipate our simulations to overpredict the melting temperature by 20−30%, as seen in other work.[28] In the literature, there have been several reports of more refined methods to determine the melting transition, such as finding the melting temperature as a function of the number of defects in the crystal,[30] finding the melting temperature for nanocrystals of increasing size and extrapolating to infinite size,[31] and introducing a solid−liquid interface in the system.[32] To explore the effect of the periodicity imposed on the crystal lattice on the melting temperature predicted by the UFF and HC force fields, we have performed simulations on an isolated nanoparticle consisting of 54 T8 molecules. The same simulation procedure was followed as for the periodic systems, and the same initial configurations were used. The systems were equilibrated for 500 ps at 100 K, and then the temperature was gradually increased by 100 K for every 100 ps until melting was observed. The translational order parameter was used to monitor the melting transition, and the results are presented in Figure 9. We note from Figure 9 that for both the UFF and HC force fields, the predicted melting temperature is significantly lower than was observed in the periodic simulations, and for the HC force field, the predicted melting temperature is now in good agreement with the experimental value.

Finally, the ability to reproduce vibrational properties has been evaluated by calculating the infrared spectrum of $H_8Si_8O_{12}$ from

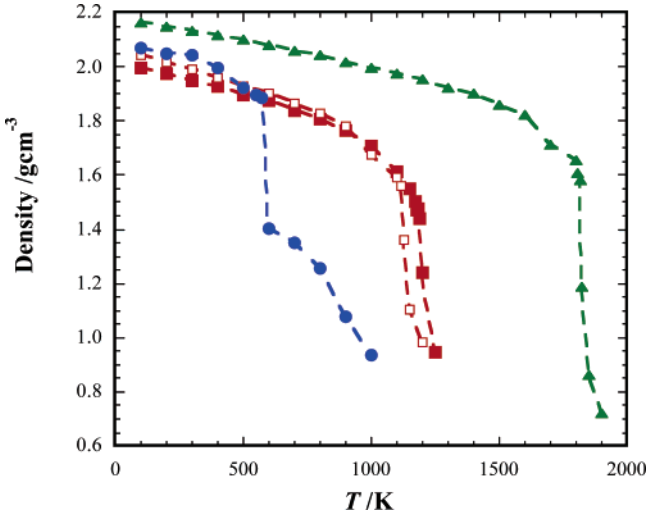

Figure 6. Density as a function of temperature for the $H_8Si_8O_{12}$ crystal obtained from the UFF (▲), Hybrid-COMPASS (■), HC w/o (χ), and CTR force fields (●).

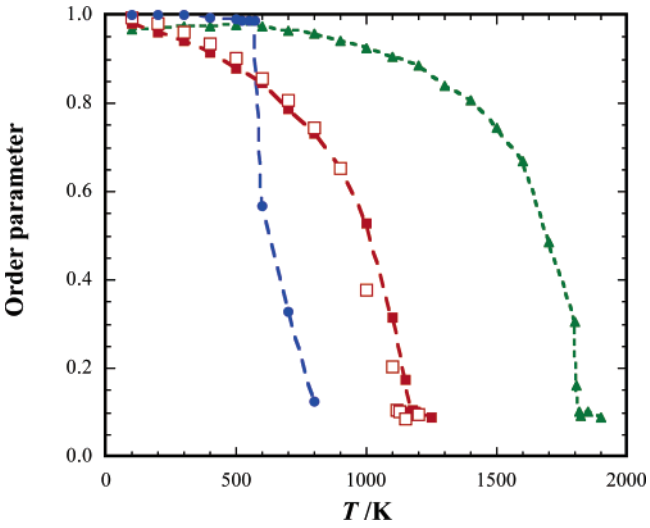

Figure 7. Translational order parameter as a function of temperature for the $H_8Si_8O_{12}$ crystal obtained from the UFF (▲), Hybrid-COMPASS (■), HC w/o (χ), and CTR force fields (●).

the Fourier transform of the current−dipole time correlation function according to

$$I(\omega) = \frac{\hbar}{4\pi^2(1 - e^{-\hbar\omega/k_BT})} \mathrm{Im}\left(\int_{-\infty}^{\infty} \langle \dot{\mu}(0)\mu(t)\rangle e^{-i\omega t}\, dt\right) \quad (31)$$

where μ is the total dipole moment of the simulated configuration. To evaluate eq 31, the force field needs to account for the fluctuations in the charge distribution in the simulated structure, therefore, we can only use the CTR force field for this calculation. We present our prediction, as well as the experimental data in Figure 10. We find that the peak positions in the simulated spectrum agree with experimental data to within less than 50 cm^{-1}, and the sequence of relative intensities matches that of the experiments well. Peak positions and relative intensities depend very sensitively on potential parameters. Changing the spacing between two spectral peaks invariably requires the adjustment of more than one potential parameter and vice versa; changing a single potential parameter affects the position and intensity of more than one spectral feature. This is why it is difficult to design interaction potentials that accurately reproduce vibrational spectra. In our experience, the

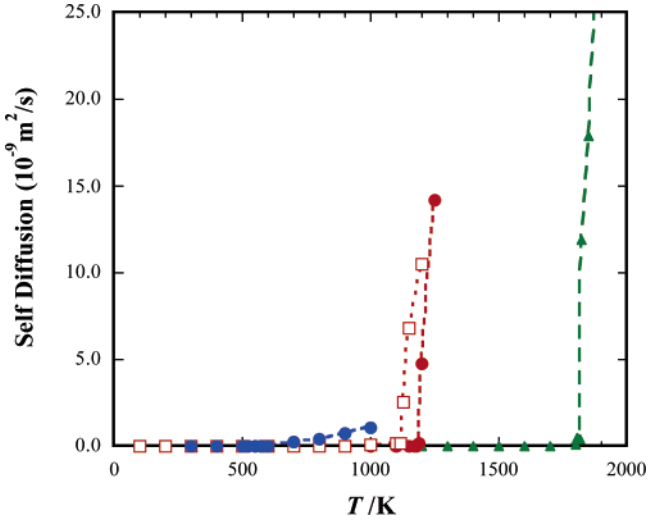

Figure 8. Self-diffusion coefficient as a function of temperature for the $H_8Si_8O_{12}$ crystal obtained from the UFF (▲), Hybrid-COMPASS (■), HC w/o (χ), and CTR force fields (●).

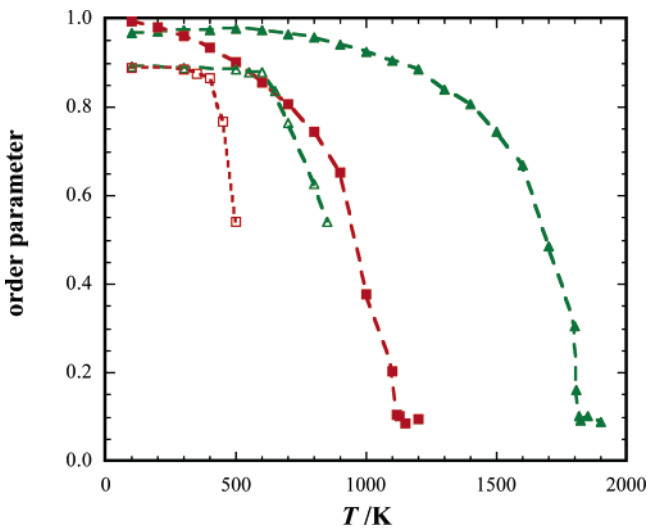

Figure 9. Translational order parameter as a function of temperature for the $H_8Si_8O_{12}$ crystal obtained from the UFF with periodic boundary conditions (▲), as a nanocrystal (△), and from the HC w/o with periodic boundary conditions (■) and as a nanocrystal (χ).

agreement between simulated and experimental spectra shown in Figure 10 can be considered as very good. Moreover, on the basis of a simulated spectrum, it is straightforward to assign the vibrational modes of motion that correspond to the various spectral peaks. This can be done by Fourier filtering the underlying atomic trajectories.[21] Accordingly, we were able to confirm that the 2280 cm^{-1} peak corresponds to the Si−H stretching mode, the 1150 cm^{-1} peak to the asymmetric Si−O−Si stretching mode, the 890 cm^{-1} peak to rattling of Si in its tetrahedral coordination shell, and the three low-frequency peaks to various Si−O−Si rocking modes. We also note that, except for the highest-frequency mode, there is a strong similarity between this spectrum and that for cristobalite silica.[21]

Conclusions

In this work, we have presented the CTR force field[33−35] for the study of POSS molecules and provided evidence that this, as well as other force fields taken from literature, can be used to obtain reliable predictions for the structural properties of systems composed of POSS molecules. The literature

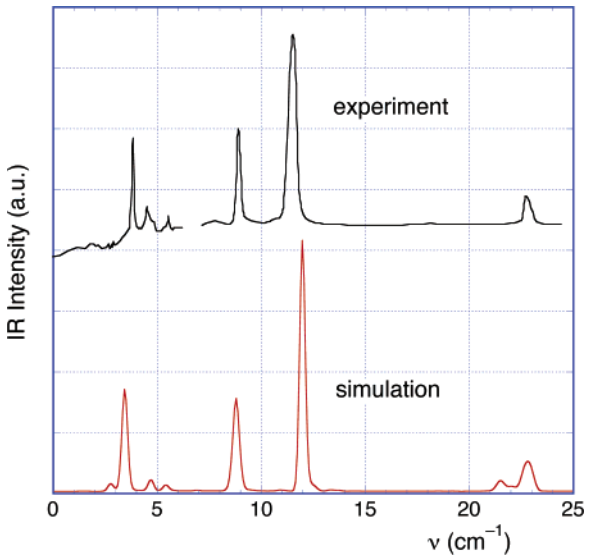

Figure 10. Comparison between experimental (top)[36,37] and simulated (bottom) infrared spectra of a POSS T-8 crystal. The simulated spectrum was obtained using the CTR force field for a defect-free crystal. The high- and low-frequency ranges of the experimental spectrum were determined by using different spectrometers, and the relationship between the relative intensities of these spectral segments is not known.

force fields compared include the universal force field,[14] the COMPASS, and the Hybrid-COMPASS force fields.[15,16,20] We predicted the structural parameters (fractional coordinates and crystal packing) of octahydrido and octamethyl silsesquioxanes and compared our predictions to available experimental data. Good agreement has been found between predicted and experimental data for all the force fields considered. We have found that the inclusion of electrostatic interactions does not significantly affect the ability of the HC force field to predict the near-range structural characteristics of silsesquioxanes, as no noticeable difference was found between the predicted properties when the electrostatic interactions were excluded. We note, however, that the melting behavior and the vibrational properties from the CTR potential are sensitive to the proper representation of the charge distribution. We have predicted the melting temperature of the perfect infinitely replicated crystal and a nanocrystal of octahydridosilsesquioxane monomers. The results provide an upper and lower bound on the predicted melting temperatures from each force field; for the CTR and HC force fields, the predicted values are in quantitative agreement with experiment. Our work provides the necessary justification for using the CTR and HC force fields for the calculation of properties of systems that contain POSS monomers via molecular simulation.

Acknowledgment. We thank Heather Barkley for performing the molecular mechanics calculations reported in Tables 6 and 7 with Materials Studio. This work is supported by the National Science Foundation (DMR-0103399). Calculations were performed at the Center for Computational Sciences at Oak Ridge National Laboratory, the National Energy Research Supercomputing Center at Lawrence Berkeley Laboratory, and on the VAMPIRE cluster at Vanderbilt University.

References and Notes

(1) Schwab, J. J.; Lichtenhan, J. D. *Appl. Organomet. Chem.* **1998**, *12*, 707.
(2) Lee, A.; Lichtenhan, J. D. *J. Appl. Polym. Sci.* **1999**, *73*, 1993.
(3) Larsson, K. *Ark. Kemi* **1960**, *16*, 215.
(4) Larsson, K. *Ark. Kemi* **1960**, *16*, 203.
(5) Larsson, K. *Ark. Kemi* **1960**, *16*, 209.
(6) Baidina, I. A.; Podberezskaya, N. V.; Alekseev, V. I.; Martynova, T. N.; Borisov, S. V.; Kanev, A. N. *J. Struct. Chem.* **1979**, *20*, 550.
(7) Koellner, G.; Muller, U. *Acta Crystallogr., Sect. C* **1989**, *45*, 1106.
(8) Tornroos, K. W.; Calzaferri, G.; Imhof, R. *Acta Crystallogr., Sect. C* **1995**, *51*, 1732.
(9) Dittmar, U.; Hendan, B. J.; Florke, U.; Marsmann, H. C. *J. Organomet. Chem.* **1995**, *489*, 185.
(10) Waddon, A. J.; Coughlin, E. B. *Chem. Mater.* **2003**, *15*, 4555.
(11) Waddon, A. J.; Zheng, L.; Farris, R. J.; Coughlin, E. B. *Nano Lett.* **2002**, *2*, 1149.
(12) Fu, B. X.; Hsiao, B. S.; Pagola, S.; Stephens, P.; White, H.; Rafailovich, M.; Sokolov, J.; Mather, P. T.; Jeon, H. G.; Phillips, S.; Lichtenhan, J.; Schwab, J. *Polymer* **2001**, *42*, 599.
(13) Xu, H. Y.; Kuo, S. W.; Lee, J. S.; Chang, F. C. *Macromolecules* **2002**, *35*, 8788.
(14) Rappe, A. K.; Casewit, C. J.; Colwell, K. S.; Goddard, W. A.; Skiff, W. M. *J. Am. Chem. Soc.* **1992**, *114*, 10024.
(15) Sun, H.; Rigby, D. *Spectrochim. Acta, Part A* **1997**, *53*, 1301.
(16) Sun, H. *Macromolecules* **1995**, *28*, 701.
(17) Li, H.-C.; McCabe, C.; Striolo, A.; Cummings, P. T.; Lee, C.-Y.; Neurock, M. *J. Phys. Chem. B* **2006**, submitted.
(18) Martin, M. G.; Siepmann, J. I. *J. Phys. Chem. B* **1998**, *102*, 2569.
(19) Accelrys Inc., *http://www.accelrys.com/mstudio/ms_modeling/index.html*.
(20) Sun, H. *J. Phys. Chem. B* **1998**, *102*, 7338.
(21) Anderson, D. C.; Kieffer, J.; Klarsfeld, S. *J. Chem. Phys.* **1993**, *98*, 8978.
(22) Frischknecht, A. L.; Curro, J. G. *Macromolecules* **2003**, *36*, 2122.
(23) Smith, W.; Forester, T. R. *J. Mol. Graphics* **1996**, *14*, 136.
(24) Allen, M. P.; Tildesley, D. J. *Computer Simulation of Liquids*; Oxford University Press: Oxford, 1987.
(25) Parrinello, M.; Rahman, A. *Phys. Rev. Lett.* **1980**, *45*, 1196.
(26) Auf der Heyde, T. P. E.; Burgi, H. B.; Burgy, H.; Tornroos, K. W. *Chimia* **1991**, *45*, 38.
(27) Bolln, C.; Tsuchida, A.; Frey, H.; Mulhaupt, R. *Chem. Mater.* **1997**, *9*, 1475.
(28) Velardez, G. F.; Alavi, S.; Thompson, D. L. *J. Chem. Phys.* **2003**, *119*, 6698.
(29) Frenken, J. W. M. *Endeavour* **1990**, *14*, 2.
(30) Agrawal, P. M.; Rice, B. M.; Thompson, D. L. *J. Chem. Phys.* **2003**, *118*, 9680.
(31) Briant, C. L.; Burton, J. J. *J. Chem. Phys.* **1975**, *63*, 2045.
(32) Morris, J. R.; Song, X. Y. *J. Chem. Phys.* **2002**, *116*, 9352.
(33) Huang, L.; Kieffer, J. *J. Chem. Phys.* **2003**, *118*, 1487.
(34) Huang, L.; Kieffer, J. *Phys. Rev. B* **2004**, *69*, 224203.
(35) Huang, L.; Kieffer, J. *Phys. Rev. B* **2004**, *69*, 224204.
(36) Bartsch, M.; Bornhauser, P.; Burgy, H.; Calzaferri, G. *Spectrochim. Acta, Part A* **1991**, *47*, 1627.
(37) Beer, R.; Burgy, H.; Calzaferri, G.; Kamber, I. *J. Electron Spectrosc. Relat. Phenom.* **1987**, *44*, 121.